

# In the Pursuit of Effective Affective Computing: The Relationship between Features and Registration

**Abstract**—For facial expression recognition systems to be applicable in the real-world, they need to be able to detect and track a previously unseen person’s face and its facial movements accurately in realistic environments. A highly plausible solution involves performing a “dense” form of alignment, where 60-70 fiducial facial points are tracked with high accuracy. The problem is that, in practice, this type of dense alignment had so far been impossible to achieve in a generic sense, mainly due to poor reliability and robustness. Instead, many expression detection methods have opted for a “coarse” form of face alignment, followed by an application of a biologically inspired appearance-descriptor such as Histogram of Oriented Gradients (HoG) or Gabor magnitudes. Encouragingly, recent advances to a number of dense alignment algorithms have demonstrated both high reliability and accuracy for unseen subjects (e.g., constrained local models). This begs the question: besides countering against illumination variation, what do these appearance-descriptors do that standard pixel representations do not? In this paper, we show that when close to perfect alignment is obtained, there is no real benefit in employing these different appearance-based representations (under consistent illumination conditions). In fact, when misalignment does occur, we show that these appearance-descriptors do work well by encoding robustness to alignment error. For this work, we compared two popular methods for dense alignment – subject-dependent active appearance models vs subject-independent constrained local models – on the task of AU detection. These comparisons were conducted through a battery of experiments across various publicly available datasets (i.e. CK+, Pain, M3 and GEMEP-FERA). We also report our performance in the recent FERA2011 challenge for the subject-independent task.

## I. INTRODUCTION

Research into affective computing has been very active over the past decade, mainly driven by social, economic and commercial interests such as marketing, human-computer-interaction, health-care, security, behavioral science, driver safety etc. The main goal of this research is to have a computer system being able to automatically detect/infer the emotional state of any person based on various modes (i.e. face, voice, body, actions) in real-time.

The majority of this work has centered on the task of facial expression detection, mostly by way of individual action unit (AU) detection. The predominant approach [1–3] to this has been to first locate and track a person’s face and facial features, derive a feature representation of the face and then classify whether or not a frame contains the AU of interest or not (see Figure 1). In terms of face alignment [4–6], this can be done either coarsely through tracking a couple of key features (i.e. Viola & Jones [7] type approach where the face and eyes are tracked) or highly accurately via a deformable model approach where a dense mesh of 60-70 points on the face is used. The latter is

desired due to their accuracy in addition to their ability to infer the 3D pose parameters (i.e. pitch, yaw and roll) and view-point normalized pixel representations (i.e. synthesize frontal view), which is ideal in situations where there is a lot of head movement, especially out-of-plane rotations. *Subject-dependent* active appearance models (AAMs) [8, 9] have been widely used in this field [5, 10–12] for those reasons but this approach requires manual labeling of key frames of the training sequence (up to 5% of frames). For applications where manually labeling of frames is prohibitive (e.g., marketing, security/law enforcement, health-care and HCI), a more generic or *subject-independent* face alignment approach is required. One such approach is the constrained local model (CLM) method developed by Saragih et al. [13]. The CLM leverages the generalization capacity of local patch experts and constraints made on the joint deformation, as provided by a point distribution model (PDM). It is similar to AAMs in that it tracks a dense mesh of points on the face that produce both shape and appearance features, but through the utilization of these patches it has been shown to work well for the subject-independent case (i.e. unseen subjects).

Once the face has been tracked, the normal convention is to apply a bank of filters, followed by a rectification step and then a pooling/subsampling strategy<sup>1</sup>. For example, the popular Histogram of Oriented Gradients (HoG) [14–17], and Gabor magnitude [16, 17] descriptors readily fit into this parametric form and have both been successfully applied to expression detection [17] (other exotic variants such as [18] are also possible, but outside the scope of this paper). These features have been widely used due to their biological relevance [19], their ability to encode edges and texture, and their invariance to illumination. More recently, Whitehill et al. [17] have argued that for the specific task of expression detection, these features provide a non-linear classification boundary when using efficient linear classifiers (e.g., linear SVM). An inherent problem with this approach, however, is the large memory and computational overheads required for training and testing. Other than cases where there is extreme illumination variation, which is unlikely for the vast majority of applications of this technology at the moment (i.e. the environment should be somewhat constant for health [6, 10] and marketing [20] applications), it begs the question: “*if we have good registration, are appearance descriptors worth the effort?*”

In addition to this central question, this paper specifically

<sup>1</sup>We have neglected the common step of contrast normalization step here, as we are primarily interested in representations that have invariance to alignment error, not illumination variation.

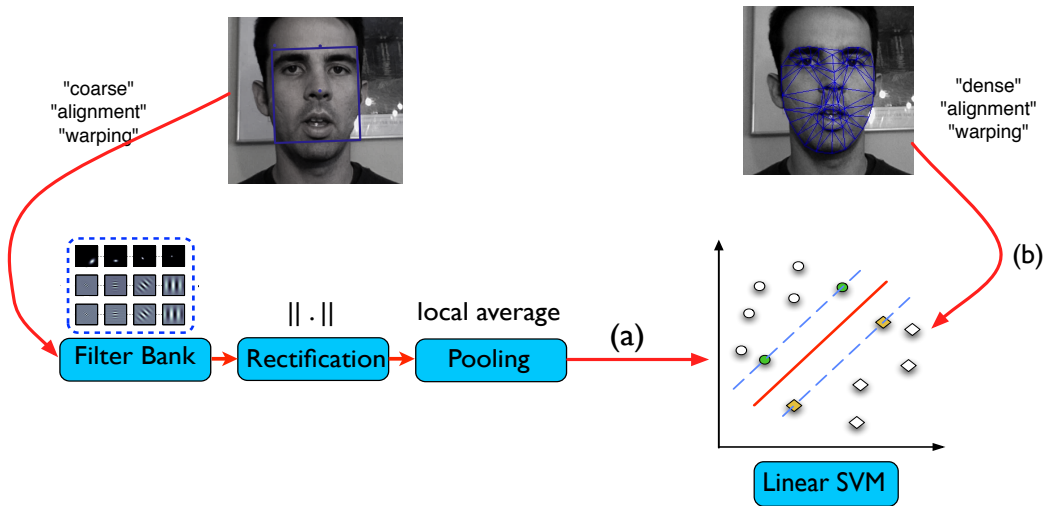


**Fig. 1:** In this paper we explore two paradigms for expression detection where a subject’s face is: (a) coarsely aligned followed by a biologically motivated descriptor (e.g., HoG or Gabor magnitudes), and (b) densely aligned using raw pixels. Both paradigms employ a linear SVM to perform classification.

looks at these other questions which are vital in the quest for effective affective computing:

- 1) What advantages do these appearance-descriptors (i.e., HoG and Gabor magnitudes<sup>2</sup>) have over pixel-based representations for the task of AU detection? When there is close to perfect alignment, is there any benefit in employing these? Does this vary between posed and spontaneous expressions? How does this change when there is poor alignment?
- 2) What is the difference between subject-dependent (AAM) and subject-independent (CLM) face alignment algorithms in terms of alignment accuracy and AU detection performance?

To quantify the effects ranging across different environments, this paper presents results for a battery of experiments across various datasets which include the posed dataset provided by the Extended Cohn-Kanade dataset (CK+) [12], spontaneous expressions using the UNBC-McMaster shoulder pain archive [6] and the M3 dataset [16], in addition to the recent GEMEP-FERA challenge [21]. We also report AU detection results obtained by the CLM in the recent Facial Expression Recognition and Analysis (FERA2011) Challenge [21] (see Section VIII).

## II. SUBJECT-DEPENDENT VS SUBJECT-INDEPENDENT DEFORMABLE IMAGE ALIGNMENT ALGORITHMS

As expressions can be subtle, alignment using a deformable model is desired so that the correspondence between various facial features and muscles contracting and controlling the face can be maintained, enhancing the ability of the classifier to detect the facial expression correctly. In addition to this, where there is quite a lot of head-movement, especially out-of-plane rotation, these models can

<sup>2</sup>In this paper, we selected only HoG and Gabor magnitudes (and not their other variants) for in-depth investigations since these have been heavily employed in the recent expression recognition literature.

be used to gain the 3D pose parameters (i.e. pitch, yaw and roll) [22], and to synthesize a uniform frontal view. In this paper, we will be comparing the *subject-dependent* active appearance model (AAM) [8,9] versus the *subject-independent* constrained local model (CLM) [13].

Subject-dependent AAMs are tuned specifically to the subject, camera conditions, and illumination of the target image sequence to be tracked [5,10,12] and are able to exhibit “human like” accuracy. This tuning is accomplished through the judicious hand labeling of key frames in the target image sequence, where up to 5% of images in a given training sequence need to be manually labelled. In applications in the fields of behavioral science and others where time can be taken to gain an accurate and objective measure, this is a viable solution.

For commercial applications where no enrollment of the subject is possible (e.g., marketing, security/law enforcement, health-care and HCI), a generic or subject-independent face alignment approach is required. Recently Saragih et al. [13] proposed the constrained local model (CLM) which is a method that leverages the generalization capacity of local patch experts and the constraint over joint deformation provided by a point distribution model (PDM). It is similar to AAMs in that it tracks a dense mesh of points on the face that produce both shape and appearance features, but through the utilization of these patches it generalises well for the subject-independent case, where the AAM does not. A description of both alignment algorithms is given in the following subsections.

### A. Active Appearance Models (AAM)

Active Appearance Models (AAMs) have been shown to be a good method of aligning a pre-defined linear shape model that also has linear appearance variation, to a previously unseen source image containing the object of interest. In general, AAMs fit their shape and appearance components

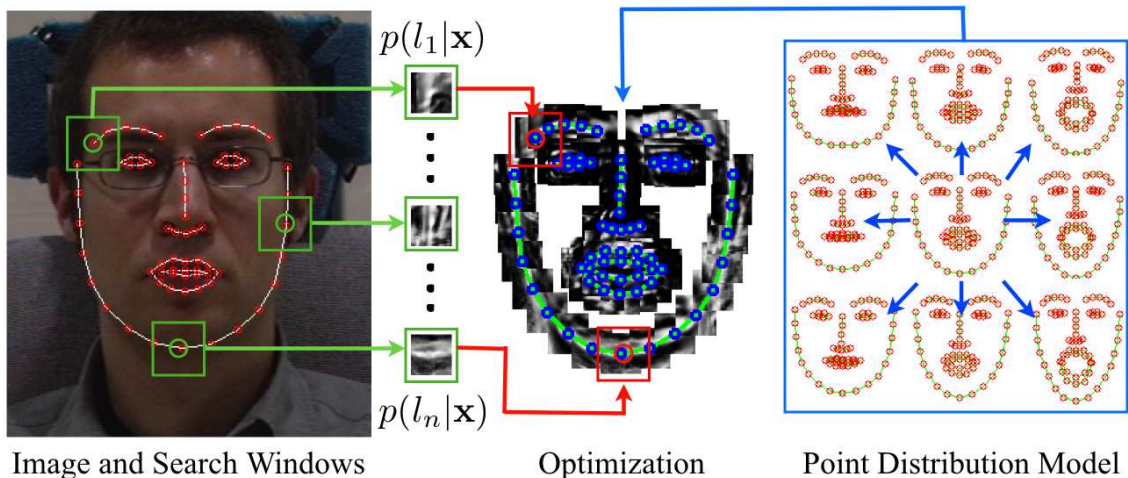


**Fig. 2:** Illustration of CLM fitting and its two components: (i) an exhaustive local search for feature locations to yield the response maps, and (ii) an optimization strategy to maximize the responses of the PDM constrained landmarks

through a gradient-descent search, although other optimization methods have been employed with similar results [8].

The shape,  $\mathbf{s}$ , of an AAM [8] is described by a 2D triangulated mesh. In particular, the coordinates of the mesh vertices define the shape  $\mathbf{s} = [x_1, y_1, x_2, y_2, \dots, x_n, y_n]$ , where  $n$  is the number of vertices. These vertex locations correspond to a source appearance image, from which the shape was aligned. Since AAMs allow linear shape variation, the shape,  $\mathbf{s}$ , can be expressed as a base shape,  $\mathbf{s}_0$ , plus a linear combination of  $m$  shape vectors  $\mathbf{s}_i$ ,

$$\mathbf{s} = \mathbf{s}_0 + \sum_{i=1}^m p_i \mathbf{s}_i, \quad (1)$$

where the coefficients  $\mathbf{p} = (p_1, \dots, p_m)^T$  are the shape parameters. These shape parameters can typically be divided into rigid similarity parameters,  $\mathbf{p}_s$ , and non-rigid object deformation parameters,  $\mathbf{p}_o$ , such that  $\mathbf{p}^T = [\mathbf{p}_s^T, \mathbf{p}_o^T]$ . Similarity parameters are associated with a geometric similarity transform (i.e. translation, rotation and scale). The object-specific parameters are the residual parameters representing non-rigid geometric variations associated with determining the object shape (e.g., mouth opening, eyes shutting, etc). Procrustes alignment [8] is employed to estimate the base shape  $\mathbf{s}_0$ .

Keyframes within each video sequence are manually labelled, while the remaining frames are automatically aligned using a gradient descent AAM fitting algorithm described in [9].

### B. Constrained Local Models (CLM)

Similarly to the AAM, we want to find the shape  $\mathbf{s}$  as in Equation 1, also known as the point distribution model (PDM). Constrained local models (CLM) [23] refer to a host of algorithms which utilize an ensemble of local detectors to determine  $\mathbf{s}$ . All of these methods have the following two goals: (i) perform an exhaustive local search for each PDM landmark around their current estimate using some kind of

feature detector, and (ii) optimize the PDM parameters such that the detection responses over all of its landmarks are jointly maximized. Figure 2 illustrates the components of the CLM fitting.

The particular instance of CLM used in this work is that proposed in [13]. The method uses linear SVMs over power normalized image patches to discriminate aligned from misaligned mesh vertex coordinates. Composing the SVM classification score with a Sigmoid function generates a likelihood map over the vertices within a local search region around its current estimate (i.e.  $p(l_i|\mathbf{x})$  in Figure 2). This allows a Bayesian treatment of the alignment problem. The advantage of using the linear SVM over more sophisticated classifiers is twofold. Firstly, it allows rapid computations of the mesh vertices' probability maps using efficient normalized cross correlation. Secondly, the linear model's limited capacity results in better generalization to unseen subject identities.

Once likelihood maps for each mesh vertex have been computed, the CLM variant in [13] uses an optimization strategy coined subspace constrained mean-shifts. By assuming the vertex likelihoods are conditionally independent given the shape, optimization proceeds by alternating two steps: 1) compute a single mean-shift update for each vertex independently of all others, and 2) project the mean-shifted vertex coordinates onto the subspace of the shape model in Equation 1. By virtue of its interpretation as an instance of the EM algorithm, this simple two step procedure is provably convergent. To encourage convergence to the global optimum in cases with gross initial misalignment, this optimization strategy is applied on a pyramid of smoothed versions of the likelihood maps, which is similar to the heuristic often used in AAM alignment but with the difference that smoothing is applied directly to the objective rather than indirectly through the image. An example of the CLM tracking an unseen face is given in Figure 3(a).

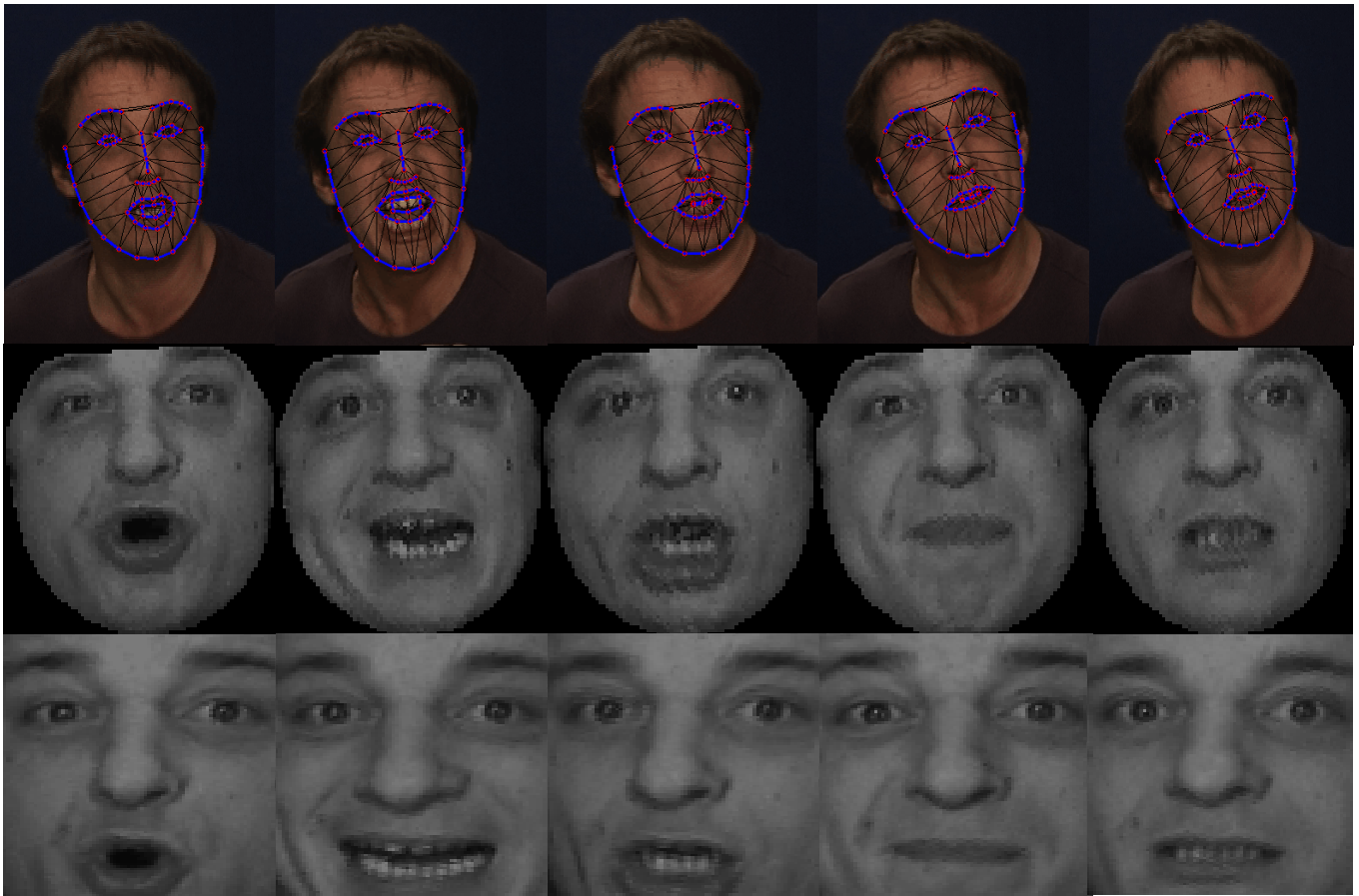


**Fig. 3:** Example of the CLM tracking a sequence from the GEMEP-FERA dataset over time: (a) Once the face is tracked we extract: (b) the canonical normalized appearance features, and (c) the similarity normalized appearance features.

### III. APPEARANCE-BASED FEATURES

Under the assumption that there will always be some degree of registration error in a target face image it is useful to explore features that give invariance to registration. Holistic invariant features are difficult to derive as one rarely has prior knowledge of how the image geometrically deforms holistically. Instead, it is simpler to adopt a strategy where a single complex holistic deformation in an image, such as those found in facial expressions, can always be broken down into multiple simple deformations (e.g., optical flow, where a single complex deformation can be defined as multiple, one for each pixel, locally constrained translations). Representing an image as a “super vector” of concatenated local region features that are invariant to simple deformations (e.g., translation), an argument can then be made that this super vector will exhibit invariance to more complex holistic registration errors.

Many different techniques for describing local image regions have been proposed in the literature. The simplest feature is a vector of raw pixel values. However, if an unknown error in registration occurs, there is an inherent variability associated with the *true* (i.e. correctly registered) local image appearance. Due to this variability, an argument can be made that these local pixel appearances are more aptly

described by a distribution rather than a static observation point. In addition to the pixel-based representations which we derive from our deformable face alignment algorithm, we investigate two popular methods in vision for obtaining distribution features that exhibit good local spatial invariance: (i) Histogram of Oriented Gradients (HoG), and (ii) Gabor magnitudes (GAB).

#### A. Pixel-Based Representations

Once we have tracked the subject’s face by estimating the shape and appearance parameters, we can use this information to derive the following features:

- **SPTS:** The similarity normalized shape,  $s_n$ , refers to the 68 vertex points in  $s_n$  for both the  $x$ - and  $y$ -coordinates, resulting in a raw 136 dimensional feature vector. These points are the vertex locations after all the rigid geometric variation (translation, rotation and scale), relative to the base shape, has been removed. The similarity normalized shape  $s_n$  can be obtained by synthesizing a shape instance of  $s$ , using Equation 1, that ignores the similarity parameters  $\mathbf{p}$ .
- **SAPP:** The similarity normalized appearance features,  $\mathbf{a}_n$ , refers to where all the rigid geometric variation (translation, rotation and scale) has been removed. It achieves this by using  $s_n$  calculated above and warps

the pixels in the source image with respect to the required translation, rotation and scale. This is the type of approach that is employed by most researchers [1, 17], as only coarse registration is required (i.e. just face and eye locations). When out-of-plane head movement is experienced some of the face is partially occluded which can affect performance, also some non-facial information is included due to occlusion. Furthermore, the shape transformation is inherently unknown since substantial variation exist between the shapes of different faces, which therefore makes the  $z$ -component of facial points difficult to estimate.

the transformation is inherently unknown (s) An example of this is shown in Figure 3(c).

- **CAPP:** The canonical normalized appearance  $\mathbf{a}_0$  refers to where all the non-rigid shape variation has been normalized with respect to the base shape  $\mathbf{s}_0$ . This is accomplished by applying a piece-wise affine warp on each triangle patch appearance in the source image so that it aligns with the base face shape. It was shown in [24] that by removing the rigid shape variation, poor performance was gained. Examples of the CAPP features is shown in Figure 3(b).

In this paper, we are interested in analyzing the change in performance of the different appearance features (SAPP and CAPP) between subject-dependent and subject-independent alignment algorithms, as well as across different feature representations (next subsections).

### B. Histogram of Oriented Gradients

Histogram of Oriented Gradients (HoG) [15], are a close relation of the descriptor in Lowe’s seminal SIFT approach [14] to code visual appearance. Briefly, the HoG method tiles the input image with a dense grid of cells, with each cell containing a local histogram over orientation bins. At each pixel, the image gradient vector is calculated and converted to an angle, voting into the corresponding orientation bin with a vote weighted by the gradient magnitude. The orientation bins were evenly spaced over  $0^\circ - 180^\circ$  (unsigned gradient). Histograms were obtained at different discrete scales using a Gaussian gradient function (in  $x$ - and  $y$ -) with the variance parameter  $\sigma^2$  defining the scale. These scale specific histograms are all concatenated into a single feature vector. Shift invariance is naturally encoded in this type of feature through the size of the cell from which the histograms are derived. The larger the cell size, the greater the shift invariance. In this work we used a cell size of  $12 \times 12$  over 3 frequencies and 4 rotations.

### C. Gabor Magnitudes

A 2D Gabor function is a complex exponential modulated by a Gaussian envelope:

$$g_{\omega, \theta}(x, y) = \frac{1}{2\pi\sigma^2} \exp\left\{ -\frac{x'^2 + y'^2}{2\sigma^2} + j\omega x' \right\}, \quad (2)$$

where  $x' = x\cos(\theta) + y\sin(\theta)$ ,  $y' = -x\sin(\theta) + y\cos(\theta)$ ,  $x$  and  $y$  denote the pixel positions,  $\omega$  represents the frequency

of the Gabor wavelet,  $\theta$  represents the orientation of the Gabor wavelet, and  $\sigma$  denotes the standard deviation of the Gaussian function (please refer to [25] on strategies for spacing the filters in the 2D spatial frequency domain for a fixed number of scales and orientations). These filters are in quadrature where the real part of the filter is even symmetric and the imaginary part of the filter is odd symmetric. When convolved with an input image the scalar magnitude value of the resultant complex response can be interpreted as the correlation matrix (i.e. distribution) of the local region (defined by  $\sigma$ ), for the image components resonating with the central frequency (defined by  $\mathbf{k}$ ) in the direction of  $\theta$ . Like HoG features, the magnitude values for each orientation and central frequency are concatenated into a vector. In this paper, we use 8 different orientations and 8 different frequencies, and employ AdaBoost to select the top 8% of the most discriminant features as a subset of the entire Gabor features space for training and testing. Please note that these optimal parameters had been selected for both Gabor magnitudes and HoG during preliminary experiments.

## IV. GEOMETRIC INVARIANCE VIA DESCRIPTORS

A laundry list of features/descriptors have now been proposed for in computer vision literature for a myriad of matching/classification tasks including expression classification. Biologically inspired descriptors such as HoG and Gabor magnitudes have proven successful in recent state of the art expression detection algorithms [16, 17]. As pointed out by Lecun et al. [26], these biologically inspired features/descriptors all share a common parametric form. This parametric form has its roots in the seminal work of Hubel and Wiesel [19] involving the study of the mammalian primary visual cortex (i.e. V1). Typically, an input image is passed through a bank of filters, followed by a rectification step, contrast normalization, and then a pooling/subsampling strategy. For example, the very popular Histogram of Oriented Gradients (HoG) [14–17], and Gabor magnitude descriptor [16, 17] readily fit into this parametric form. Recently, variants of this parametric have been explored [18, 27, 28], with impressive performance being obtained for a number of vision classification tasks. For example, Serre et al. [18] demonstrated that the tuning properties of a majority of cortical cells in the visual cortex could be captured by selecting the parameter values that correspond to a host of different visual stimuli.

The performance of human vision is obviously far superior to that of current computer vision systems at the moment, so there is a valid argument to be had in emulating biological processes. However, this explanation is largely unsatisfying from an engineering perspective for understanding why these features are useful. As Berg & Malik [29] elegantly point out, one useful consequence of treating the positive and negative components of oriented edge responses separately (or rectifying them) is that information about zero crossings is not lost under blurring. Instead of blurring the signal response around a zero crossing to zero, the positive and negative responses are both blurred over the area, retaining the information that

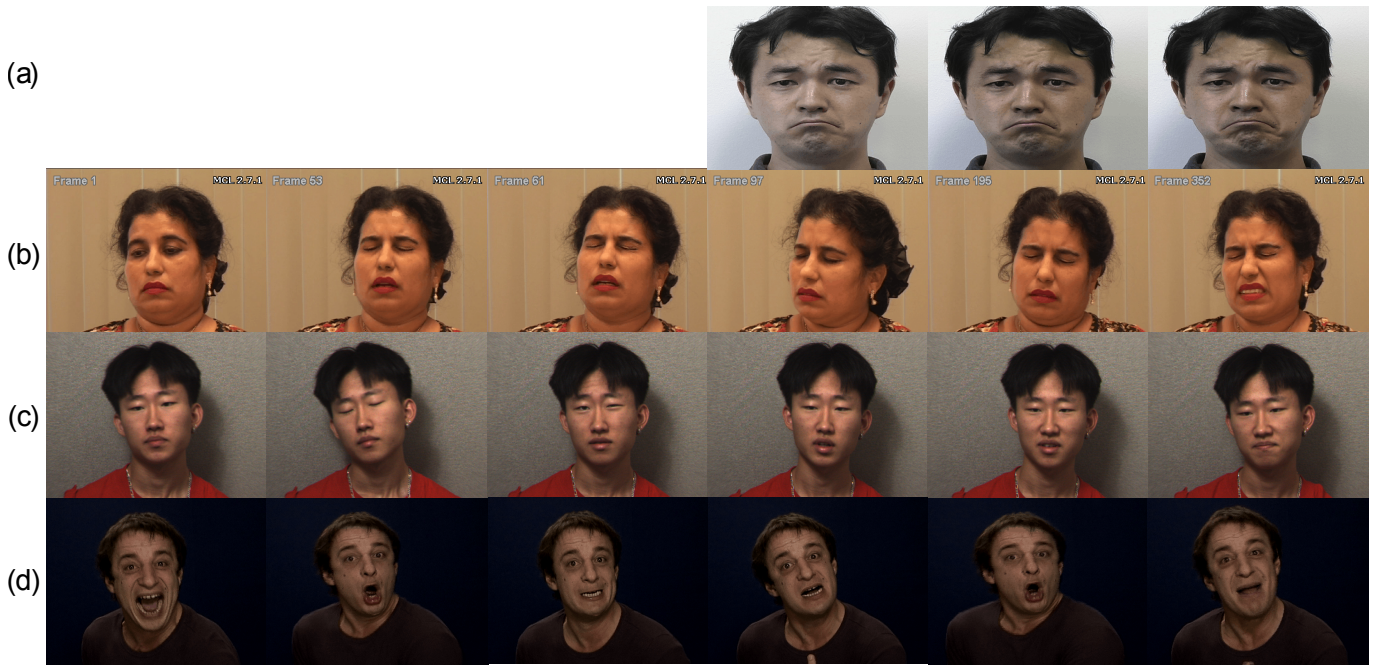


**Fig. 4:** Examples of the four datasets that we used in this paper: (a) The Extended Cohn-Kanade dataset (CK+), (b) the UNBC-McMaster Shoulder Pain Archive, (c) the M3 database, and (d) the GEMEP-FERA dataset.

there was a zero crossing, but allowing uncertainty as to its position. This non-linear process enables an encoding that is able to handle much greater tolerance than traditional pixel representations to geometric misalignment. Lecun et al. [26] refers to this blurring process more generically as “pooling”, pooling operations other than blurring (e.g., taking the maximum of a local spatial cell) have been explored in [18, 27, 28].

## V. EXPERIMENTAL SETUP AND DATASETS

### A. Experimental Setup

In this paper, all experiments were for the task of subject-independent action unit (AU) detection. These experiments were to: 1) investigate the role of biologically inspired features (Gabor and HoG features) across various levels of registration accuracy and compare them to pixel representations, and 2) compare the registration accuracy between subject-dependent (AAM) and subject-independent face registration algorithms and their subsequent performance for AU detection. To facilitate this, we conducted these experiments across four common facial expression datasets (see subsection V-B).

Once we tracked the face and extracted representative facial features (see Sections II and III), the classification of these AUs was performed via a linear support vector machine (SVM). Support vector machines (SVM) are an effective method for AU classification and they are used in many facial expression systems [17, 30–32]. In this paper, we used a one-vs-all linear two-class SVM (i.e. AU of interest vs non-AU of interest) in all experiments. For the training of the SVMs, all frames which were manually labelled by expert FACS coders to contain the AU of interest were used as positive examples, regardless whether it occurred with other AUs or

**TABLE I:** In selecting negative training examples, the AUs which are in close proximity with one another had been categorized into the following pools as the differences between them are quite subtle (e.g., for AU1, we did not include any frames which had AU2 nor AU4 in the negative pool).

AU Pool	Facial Region	AUs Involved
1	<i>upper face</i>	1–2–4
2	<i>middle face</i>	6–7–9–10
3	<i>lower face</i>	12–15–17–18–25–26

alone. The frames that did not have the AU of interest in them were used as negative examples<sup>3</sup>.

Training and testing was conducted using a leave-one-subject-out strategy, so as to maximize the amount of training and testing data. It is also worth noting that all AAM experiments were subject-dependent (i.e., approximately 5% of all images in a training given sequence were used to train an AAM to track that sequence). The CLM used in these

<sup>3</sup>There is the following exception, if similar AUs occurred - these were not used in the negative example pool. Please refer to Table I for our AU pooling strategy. Please also note that this intuitive strategy have not been empirically proven to provide optimal AU detection performance.

experiments had NOT seen any of the images in any of the datasets (i.e. completely generic).

In order to predict whether or not a video frame contained an AU, the output score from the SVM was used. As there are many more frames with no behavior of interest than frames containing a behaviour of interest, the overall agreement between correctly classified frames can skew the results somewhat. As such, we used the receiver-operator characteristic (ROC) curve, which is a more reliable performance measure. This curve is obtained by plotting the hit-rate (true positives) against the false alarm rate (false positives) as the decision threshold varies. From the ROC curve, we used the area under the ROC curve ( $A'$ ), to assess the performance. The  $A'$  metric ranges from 0.5 (pure chance) to 1 (ideal classification). An upper-bound on the uncertainty of the  $A'$  statistic was obtained using the formula  $s = \sqrt{\frac{A'(100-A')}{\min\{n_p, n_n\}}}$  where  $n_p, n_n$  are the number of positive and negative examples respectively [17, 33]. We chose this approach over the F1 metric as the latter relates only to the maximum F1 score on the precision-recall curve which does not give an indication of the generalised performance for different thresholds<sup>4</sup>.

## B. Datasets

1) *The Extended Cohn-Kanade Database:* In this paper we used the extended Cohn-Kanade (CK+) database [12], which contains 593 sequences from 123 subjects. The image sequences vary in duration (i.e. 10 to 60 frames) and incorporate the onset (which is also the neutral frame) to peak formation of the facial expressions (see Figure 4(a)). For the 593 posed sequences, full FACS coding of the peak frames is provided. Approximately fifteen percent of the sequences were comparison coded by a second certified FACS coder. Inter-observer agreement was quantified with coefficient kappa, which is the proportion of agreement above what would be expected to occur by chance [34]. The mean kappas for inter-observer agreement were 0.82 for action units coded at apex and 0.75 for frame-by-frame coding. An inventory of the AUs we used in this experiment are given in Table II.

2) *The UNBC-McMaster Shoulder Pain Archive:* The UNBC-McMaster Shoulder Pain Expression Archive contains video of the faces of adult subjects (129 subjects - 63 male, 66 female) with rotator cuff and other shoulder injuries. In the portion released by Lucey et al. [6], 200 video sequences spanning 25 subjects were recorded of their faces while they moved their affected (these subjects had various shoulder injuries) and unaffected shoulders. In this dataset considerable head movement occurs during the sequence and the video sequences have various durations, with sequences lasting from 90 to 700 frames. Within these sequences, the patient may display various expressions multiple times (of which all AUs had been fully FACS coded). In total there were over 48000 frames used. An inventory of the AUs used

**TABLE II:** AU inventory of the number of instances of AUs that were present in the various datasets used in this paper.

AU	CK+	Pain	RUFACS	GEMEP
1	173	–	16319	1600
2	116	–	13722	1631
4	191	1074	2204	1356
6	122	5557	7980	1808
7	119	3366	7980	2123
9	–	423	–	–
10	–	525	5471	2034
12	111	6887	28017	2725
15	89	–	4232	1026
17	196	–	8383	822
18	–	–	–	419
25	287	2407	28865	812
26	48	2093	19782	499
43	–	2434	–	–

for these experiments is also given in Table II. An example of the dataset is given in Figure 4(b). For full details of this freely available dataset please see [6].

3) *M3 Database:* The spontaneous M3 [16] facial expression database was recorded from a hundred participants of a false-opinion paradigm. This paradigm proved effective at evoking a plethora of emotion related facial expressions, where subjects first fill out a questionnaire regarding their opinions about a social or political issue, and then attempted to deceive an experienced interviewer for monetary gains. For each subject, approximately two minutes of video was recorded, which was coded by two separate certified FACS coders. As these expressions are spontaneous, a mixture of AUs tend to overlap with one another (i.e. co-occurrence), at varying levels of intensity. Other facets of the spontaneous nature include speech-related mouth movements and out-of-plane head rotations. An example of the dataset is given in Figure 4(c). Ground truth FACS coding was provided by expert coders. Data from 28 of the subjects was available for our experiments. In particular, we divided this dataset into 17 subjects for training (97000 frames) and 11 subjects for testing (67000 frames). For the other 3 datasets, we conducted our experiments using a leave-one-subject-out strategy for training and testing. An inventory of the AUs used in this experiment is given in Table II.

4) *The GEMEP-FERA Database:* The GEMEP-FERA database [21] contains audio-visual recordings of 10 actors expressing a total of 15 emotions together with a variety of AUs which had been FACS coded. In all of these recordings, the actors were instructed to utter meaningless phrases (such as the sustained vowel ‘aaa’) with the aid of a professional director. The key difference between this dataset with the CK+ and UNBC-McMaster Shoulder Pain Archive is that expressions had been displayed in the presence of speech, which generated a substantial amount of rigid head and body motion. An example of the dataset is given in Figure 4(d). In our experiments, we focused on the following AUs: {1

<sup>4</sup>We however did use the F1 metric in reporting our AU performance in the FERA2011 challenge however.

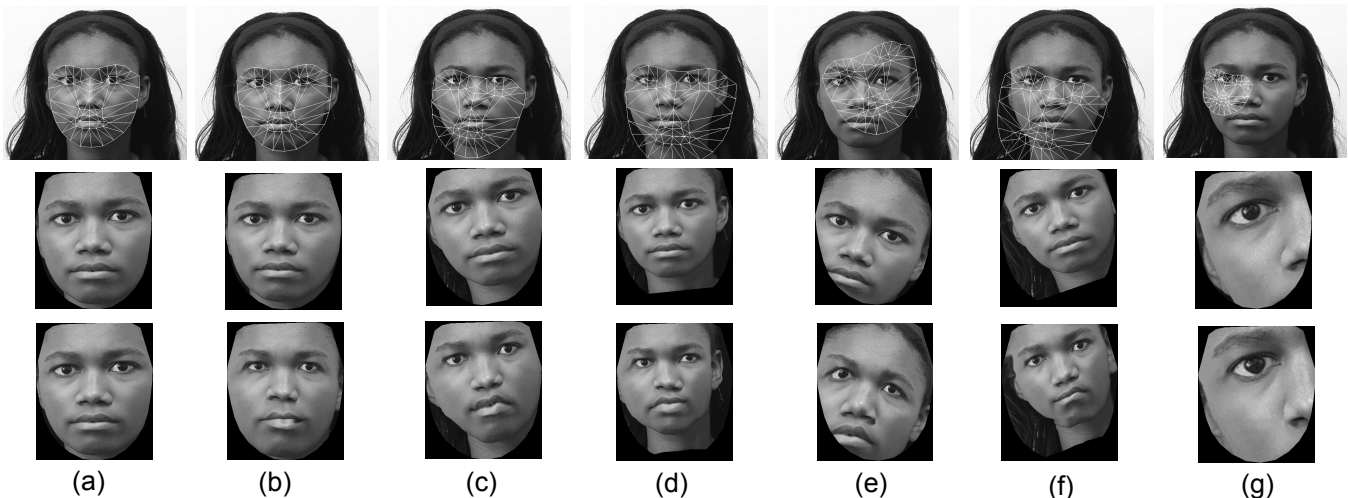


**Fig. 5:** In our experiments, we compared the SAPP (row 2) and CAPP (row 3) features from the AAM across various geometric noise levels, which is symptomatic of poor registration in subject independent algorithms: (a) ideal tracking, (b) 5 RMS-PE, (c) 10 RMS-PE, (d) 15 RMS-PE, (e) 20 RMS-PE, (f) 25 RMS-PE, and (g) 30 RMS-PE. From this it can be seen when the amount of noise is increased, the piece-wise affine warp which synthesizes the CAPP image causes significant deformation to the face which is a much noisier representation than the SAPP image.

2 4 6 7 10 12 17}. The number of these AUs are given in Table II.

## VI. EXPERIMENT I: THE ROLE OF FEATURES

We had two main interests here: 1) comparing different AAM pixel representations across noise levels (SAPP vs CAPP), and 2) comparing these pixel representations against biologically inspired features (i.e., HoG and Gabor magnitudes). To facilitate these goals, we added various amounts of geometric noise to the test images. To do this, the similarity normalized base template had an inter-ocular distance of 50 pixels. For a fair comparison, we took into account differing face scales between testing images. This is done by first removing the similarity transform between the estimated shape and the base template shape and then computing the root-mean-squared pixel-error (RMS-PE) between the 68 points. We obtained the poor initial alignment by synthetically adding affine noise to the ground-truth coordinates of the face. We then perturbed these points with a vector generated from white Gaussian noise. The magnitude of this perturbation was controlled to give a desired RMS-PE from the ground-truth coordinates (which were the AAM tracked landmarks). During learning, the initially misaligned images were defined to have between 5-30 RMS-PE. This range of perturbation was chosen as it approximately reflects the range of alignment error that can be experienced using subject independent face alignment algorithms. Examples of the poor tracking are given in Figure 5. In our experiments, all training images were clean (i.e. zero noise) and they were tested across different noise levels (i.e. 5-30 RMS-PE). After all images were registered, they were downsampled to  $48 \times 48$  pixels. As can be seen in Figure 5(c), when the amount of noise is increased, the piece-wise affine warp which synthesizes the CAPP image causes significant deformation to the face (observe the lip area in Figure 5(c)) which is a

much noisier representation than the SAPP image. As this is the case, all HoG and Gabor features were calculated on the SAPP pixel representations. The results for these experiments are given in Figure 6.

As can be seen, there is a gradual drop-off in performance as the amount of noise is increased across all the datasets (a-d). The first thing to note is the performance of both the AAM representations (SAPP=black, CAPP=blue). As observed from the two pixel representations, the performance is very similar so there is little difference between these two at the zero-noise condition, but it was observed that the performance CAPP appeared to deteriorate more rapidly than SAPP on the CK+ and Pain experiments. What is interesting though, is that when the amount of noise was increased, the biologically-inspired features outperform the pixel representations (especially for the CK+ Figure 6 (a) and M3 datasets Figure 6 (c)). This supports the reason for the combination of coarse registration and a biologically-inspired descriptor is widely used in literature [16]. As the amount of head motion present in the majority of applications this system is applied on can be considered to be limited, having a coarse registration (noise from 0-15 RMS-PE) would produce only slight degradation in performance when these features are employed.

## VII. EXPERIMENT II: AAM VS CLM

### A. Comparing Alignment Accuracy

In comparing the alignment accuracy of both the AAM and CLM to manually landmarked images, we first normalized all tracked AAM and CLM points and manual landmarks for similarity to a common mesh size and rotation, with a inter-ocular distance of 50 pixels and aligned to the centre of the eye coordinates. For the CK+ database, we compared against 393 manually landmarked images; for the UNBC-McMaster Pain database, we compared against 2584

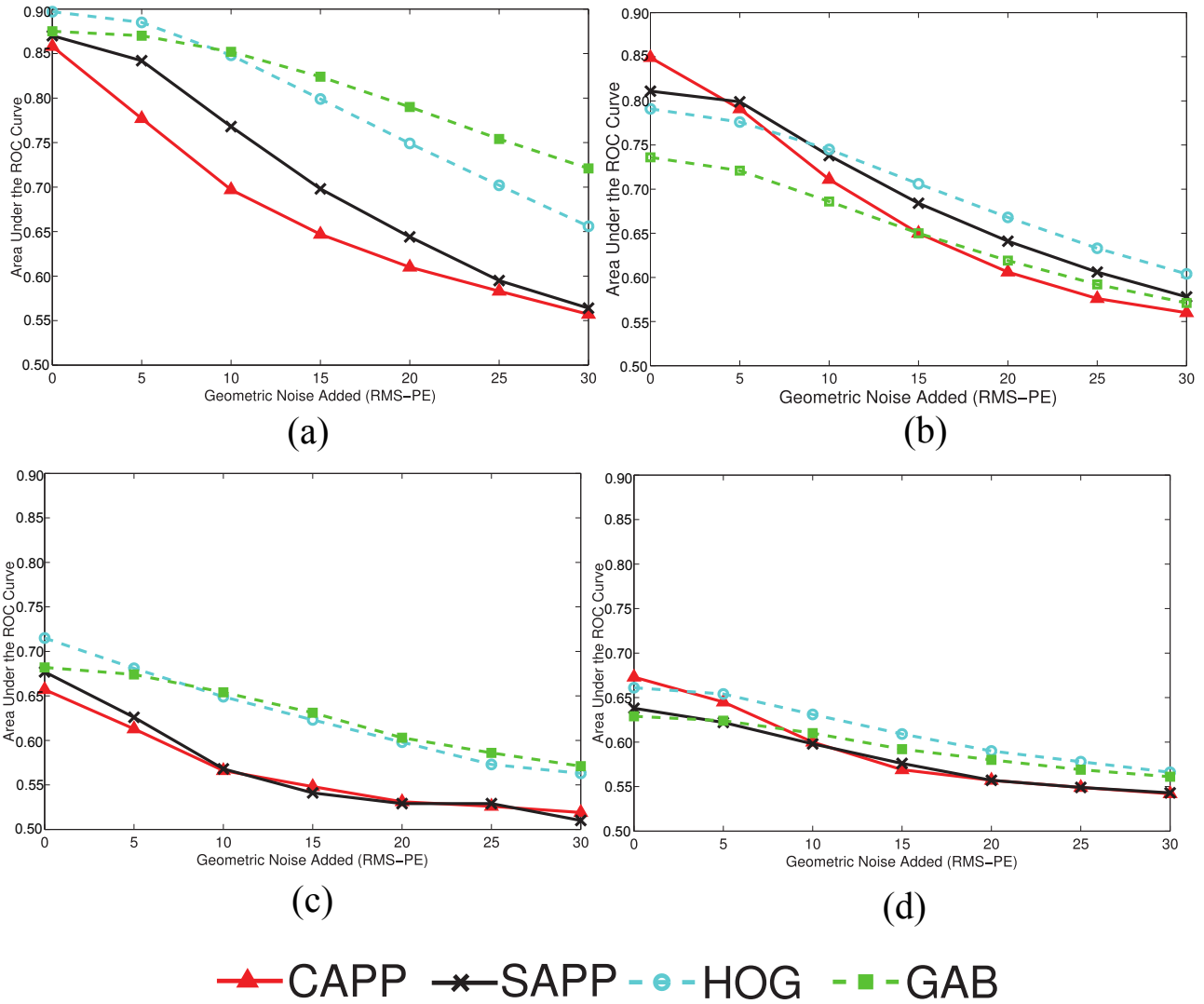


**Fig. 6:** Plots showing the average AU detection performance across all noise levels for the pixel (PIX), histogram of Oriented gradients (HoG) and Gabor features (GAB) for the following datasets: (a) CK+, (b) the UNBC-McMaster Pain Archive, (c) M3 and (d) GEMEP-FERA. Detection performance was evaluated using the weighted mean  $A^*$  proportional to the number of positive examples (i.e. the higher the number of positive examples the higher the weighting).

manually landmarked images, for M3 we compared against 1990 images; and for the GEMEP we compared against 963 manually landmarked images. The alignment curves are given in Figure 7. As can be seen for the CK+ dataset (Figure 7(a)), nearly all of the AAM landmarks are within 2 pixels RMS error of the manual landmarks, which is negligible when one considers that this is based on a distance of 50 pixels between the center of the eyes. The CLM is within 5 pixels which is also very accurate.

For the more visually complex datasets such as the UNBC-McMaster Pain Archive (Figure 7 (b)), the AAM performed very well while the CLM performance was not as good which highlights the benefit of a subject-dependent approach. However, as the majority of images were tracked within 10 pixels, which is a reasonable result, considering the relatively significant quantities of head motion in the dataset. Similar findings can be found for both the M3 (Figure 7 (c)) and

GEMEP-FERA (Figure 7 (d)) datasets. Using the results in the previous section, it can be seen that even though there was a drop-off in performance across these noise levels, the discrepancy between the different pixel representations and HoG and Gabor features would be minimal.

### B. Comparing AU Detection Performance

The experiments in Section VI were conducted using subject-dependent AAMs which provide ideal face registration. These subject-dependent AAMs were tuned specifically to a particular subject to counter for high appearance variabilities such as illumination, pose and camera conditions. The drawback of this is that alignment accuracy deteriorates once the target population is large, and having to learn specific models for each available subject becomes infeasible. On the other hand, subject-independent CLMs are well-suited to handle the problem of subject-dependence as they are able to generalise well to unseen subjects. The trade-off, however, is

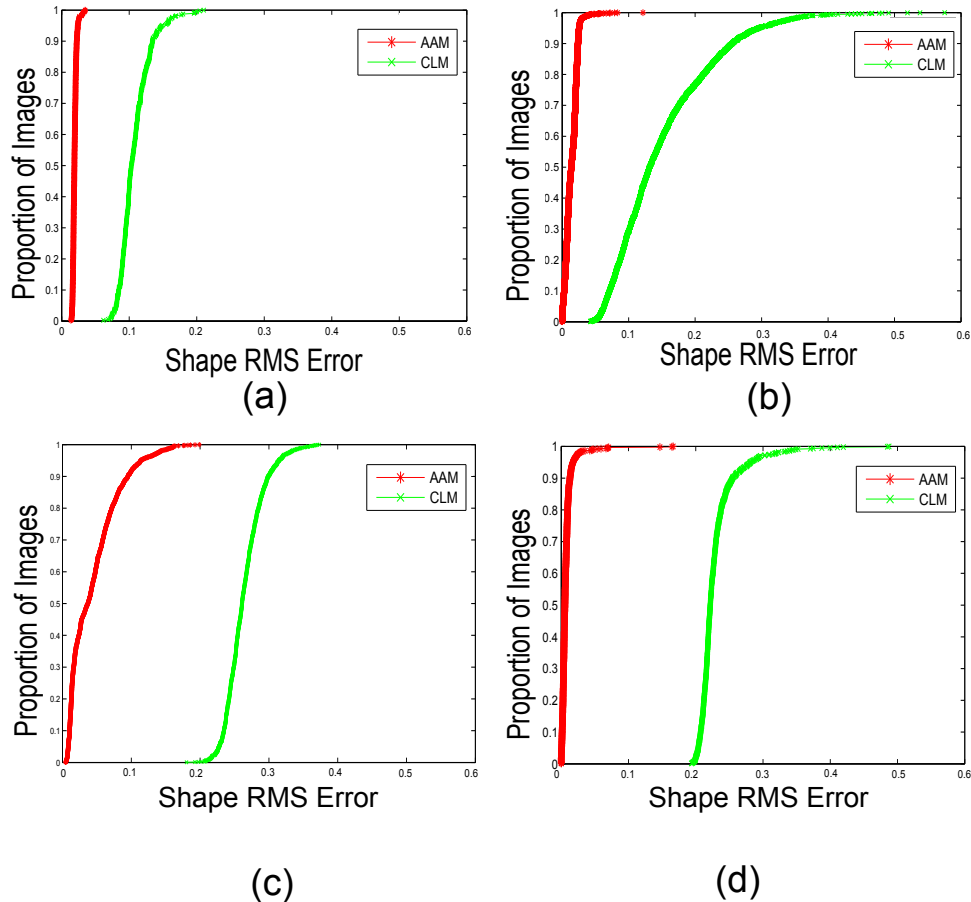


**Fig. 7:** Fitting curves comparing the registration accuracy between the AAM and CLM across the: (a) CK+, (b) UNBC-McMaster Pain Archive, (c) M3, and (d) GEMEP-FERA datasets. Shape RMS error is presented as a ratio with respect to inter-ocular distance (50 pixels).

that CLMs exhibit a deterioration in alignment accuracy as compared to AAMs. The experiments in this section evaluate the role of features in CLM-derived pixel representations, and determine if the implementation of such features could improve AU detection performances to ideal AAM levels.

Similar to the synthetic experiments in Section VI, PIX (CAPP) was compared against HoG and GAB across all four datasets, but this time only clean test images were utilized. Experimental results illustrated in Figure 8 once again suggest that little benefit could be obtained from utilizing HoG and GAB on CLM-derived pixel representations at 0 RMS-PE. Although certain appearance-descriptors may be relatively “cheap” to compute (e.g., local binary pattern operators), but these analyses provide additional insights into their fundamental operations, and could serve as a platform to inspire future methods in either appearance-descriptors or dense facial alignment methods.

For AU detection (Figure 9), the performance of the CLM was very similar (within 3%) to the AAM in all but the UNBC-McMaster Pain Archive. In this archive, there was substantially more rigid head motion as compared to the other three datasets, which indicates that the CLM does provide similar face alignment performances to the AAM when out-of-plane rigid head motion is kept minimal, but it

is still outperformed by the AAM in aligning the face from a synthesized frontal view.

## VIII. FERA2011 CHALLENGE RESULTS

Motivated by these findings, we decided to participate in the recent Facial Expression Recognition and Analysis Challenge (FERA2011) [21], as an opportunity to evaluate our CLM system. In this challenge, participants were assigned the task of automatically recognising a total of 12 Action Units (AU 1 2 4 6 7 10 12 15 17 18 25 26) from the GEMEP-FERA testing partition. Here, half of the test subjects were the same as the subjects in the training partition. Our CLM (CAPP) AU detector was trained on using examples from the GEMEP-FERA training partition and the CK+ dataset based on a leave-one-subject-out strategy. AU detection thresholds were obtained where the maximum F1-scores occurred in the respective precision-recall curves. The AU classification rates achieved in the challenge are presented in Table III. In comparison to the baseline system [21] (which employed local binary pattern operators in combination with a RBF kernel SVM), our CLM system achieved much better results. The poor detection of AU 6 and 25, however, was somewhat puzzling. The poor detection of AU 25 could be attributed to poor tracking of the mouth region, especially on the lips

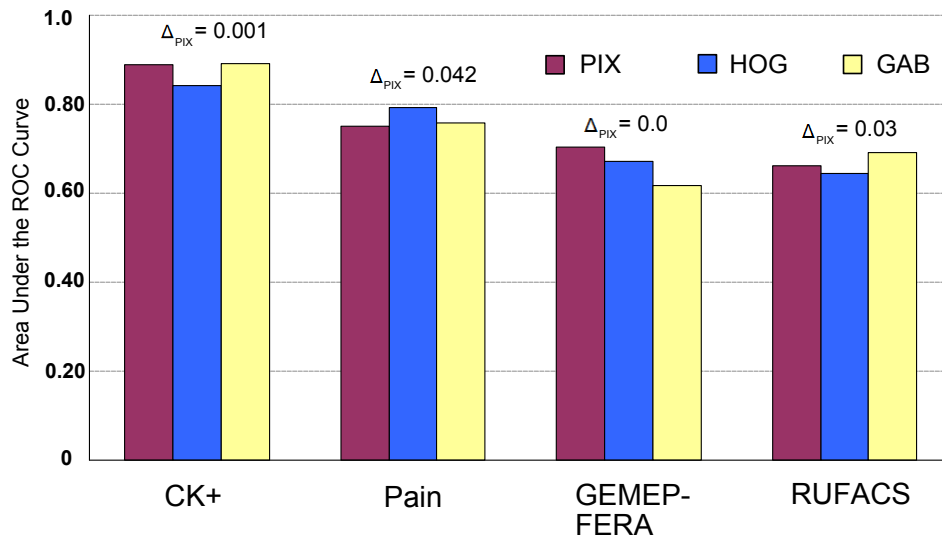


**Fig. 8:** Comparison of CLM-derived pixel representations (PIX) vs Histogram of Oriented Gradients (HoG) and Gabor magnitudes (GAB) in AU detection on the four facial expression datasets. Detection performance was evaluated using the weighted mean  $A'$  scores averaged across all AUs.  $\Delta_{PIX}$  represents the amount of benefit gained from using either HoG or GAB features over PIX. .

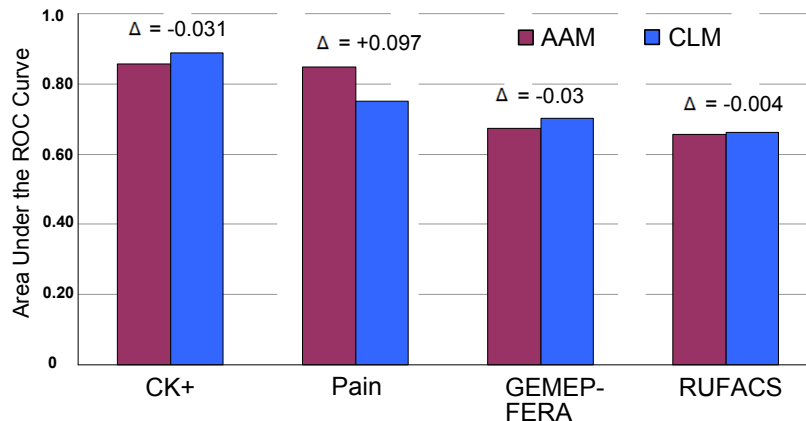


**Fig. 9:** Comparison of the overall performance between subject-dependent AAMs vs subject-independent CLMs in AU detection performance on the four facial expression datasets. Detection performance was evaluated using the weighted mean  $A'$  scores averaged across all AUs.  $\Delta$  represents the difference in detection accuracy between the AAM and CLM. .

(since subjects were constantly speaking). Registration-error of key points at the mouth region could thus propagate through to the cheek region (AU 6), and subsequently cause incorrect pixel-warping due to the poorly-tracked mouth region; and hence explain the poor detection of AU 6.

## IX. CONCLUSION

The field of affective computing is fast maturing (the recent FERA2011 challenge is indicative of this) and fully automatic facial expression recognition systems will be a reality soon. However, a major hurdle in the pursuit of achieving this is the accuracy and robustness of a generic (i.e. subject-independent) face and facial feature tracker where a large number (e.g., 60 or 70) of fiducial points on the face image are accurately detected. This paper illustrated that with the advent of subject-independent face alignment methods such as Constrained Local Models (CLM), this goal is becoming closer as the accuracy that it can achieve is comparable to the subject-dependent active appearance

models (AAM). With this high accuracy achieved, it was also shown that the benefit of employing biologically-inspired features over pixels is nullified (given that illumination conditions are known and reasonably consistent) as these features essentially provides shift-invariance which is not required when close to ideal registration is achieved. This was demonstrated over four publicly available datasets, and motivated by these results the usefulness of the CLM was also demonstrated in the recent FERA2011 challenge which performed very well in the subject-independent section. This bodes well for the future of this technology as it shows that we are getting closer to the lofty goal of having “effective” affective computing.

Future work will look into the problem of making the classifier invariant in the temporal domain which has the potential to improve AU and expression detection performance. Once these areas can be fully explored and quantified, a better understanding on which approach can be best used

**TABLE III:** GEMEP-FERA dataset AU Testing Partition results (F1-Scores) achieved by the CLM in the FERA2011 challenge. Baseline scores [21] are also shown.  $\mu$  represents the mean.

AU	CLM System	Baseline System
1	<b>0.78</b>	0.63
2	<b>0.72</b>	0.68
4	<b>0.43</b>	0.13
6	<b>0.66</b>	0.85
7	<b>0.55</b>	0.49
10	<b>0.47</b>	0.45
12	<b>0.78</b>	0.77
15	<b>0.16</b>	0.08
17	<b>0.47</b>	0.38
18	<b>0.45</b>	0.13
25	<b>0.31</b>	0.80
26	<b>0.54</b>	0.37
$\mu$	<b>0.53</b>	0.45

for a particular application can be made.

#### REFERENCES

- [1] M. Bartlett, G. Littlewort, M. Frank, C. Lainscsek, I. Fasel, and J. Movellan, "Automatic Recognition of Facial Actions in Spontaneous Expressions," *Journal of Multimedia*, 2006.
- [2] T. Wu, M. Bartlett, and J. Movellan, "Facial expression recognition using gabor motion energy filters," Machine Perception Laboratory, University of California San Diego, Tech. Rep.
- [3] A. Ashraf, S. Lucey, and T. Chen, "Re-Interpreting the Application of Gabor Filters as a Manipulation of the Margin in Linear Support Vector Machines," *IEEE Transactions on Pattern Analysis and Machine Intelligence (in press)*, 2010.
- [4] J. Whitehill and C. Omlin, "Haar features for faces au recognition," in *Seventh IEEE International Conference on Automatic Face and Gesture Recognition (FG'06)*, 2006, pp. 97–101.
- [5] S. Lucey, I. Matthews, C. Hu, Z. A. F. de la Torre, and J. Cohn, "AAM Derived Face Representations for Robust Facial Action Recognition," in *Proceedings of the International Conference on Automatic Face and Gesture Recognition*, I. Matthews, Ed., 2006, pp. 155–160.
- [6] P. Lucey, J. Cohn, K. Prkachin, P. . Solomon, and I. Matthews, "PAINFUL DATA: The UNBC-McMaster Shoulder Pain Expression Archive Database," in *IEEE International Conference on Automatic Face and Gesture Recognition*, 2011.
- [7] P. Viola and M. Jones, "Rapid Object Detection using a Boosted Cascade of Simple Features," in *Proceedings of the International Conference on Computer Vision and Pattern Recognition*, vol. 1, 2001, pp. 511–518.
- [8] T. Cootes, G. Edwards, and C. Taylor, "Active Appearance Models," *IEEE Transactions on Pattern Analysis and Machine Intelligence*, vol. 23, no. 6, pp. 681–685, 2001.
- [9] I. Matthews and S. Baker, "Active appearance models revisited," *International Journal of Computer Vision*, vol. 60, no. 2, pp. 135–164, 2004.
- [10] A. Ashraf, S. Lucey, J. Cohn, K. M. Prkachin, and P. Solomon, "The Painful Face II– Pain Expression Recognition using Active Appearance Models," *Image and Vision Computing*, vol. 27, no. 12, pp. 1788–1796, 2009.
- [11] A. Asthana, J. Saragih, M. Wagner, and R. Goecke, "Evaluating AAM Fitting Methods for Facial Expression Recognition," in *Proceedings of the International Conference on Affective Computing and Intelligent Interaction*, 2009.
- [12] P. Lucey, J. Cohn, T. Kanade, J. Saragih, Z. Ambadar, and I. Matthews, "The extended cohn-kanade dataset (ck+): A complete dataset for action unit and emotion-specified expression," in *Proceedings of the IEEE Workshop on CVPR for Human Communicative Behavior Analysis*, 2010.
- [13] J. Saragih, S. Lucey, and J. Cohn, "Face Alignment through Subspace Constrained Mean-Shifts," in *Proceedings of the International Conference on Computer Vision (ICCV)*, 2009.
- [14] D. G. Lowe, "Distinctive Image Features from Scale-Invariant Key-points," *International Journal of Computer Vision*, vol. 60, no. 2, pp. 91–110, November 2004.
- [15] N. Dalal and B. Triggs, "Histograms of Oriented Gradients for Human Detection," in *IEEE International Conference on Computer Vision and Pattern Recognition*, 2005.
- [16] M. Bartlett, G. Littlewort, M. Frank, C. Lainscsek, I. Fasel, and J. Movellan, "Automatic Recognition of Facial Actions in Spontaneous Expressions," *Journal of Multimedia*, vol. 1, no. 6, pp. 22–35, 2006.
- [17] J. Whitehill, G. Littlewort, I. Fasel, M. Bartlett, and J. Movellan, "Towards Practical Smile Detection," *IEEE Transactions on Pattern Analysis and Machine Intelligence*, vol. 31, no. 11, pp. 2106–2111, 2009.
- [18] T. Serre, L. Wolf, S. Bileschi, M. Riesenhuber, and T. Poggio, "Robust Object Recognition with Cortex-Like Mechanisms," in *IEEE Transactions on Pattern Analysis and Machine Intelligence*, vol. 29, no. 3, Mar. 2007.
- [19] D. Hubel and T. Wiesel, "Receptive Fields, Binocular Interaction and Functional Architecture in the Cat's Visual Cortex," *Journal of Physiology*, vol. 160, pp. 106–154, 1962.
- [20] M. Yeasin, B. Bulot, and R. Sharma, "Recognition of facial expressions and measurement of levels of interest from video," *IEEE Transactions on Multimedia*, vol. 8, no. 3, pp. 500–508, Jun. 2006.
- [21] M. Valstar, B. Jiang, M. Mehu, M. Pantic, and K. Scherer, "The First Facial Expression Recognition and Analysis Challenge," in *Proceedings of the IEEE International Conference on Automatic Face and Gesture Recognition*.
- [22] J. Xiao, S. Baker, I. Matthews, and T. Kanade, "Real-Time Combined 2-D +3-D Active Appearance Models," in *Proceedings of IEEE Conference on Computer Vision and Pattern Recognition*, 2004, pp. 535–542.
- [23] D. Cristinacce and T. Cootes, "Feature detection and tracking with constrained local models," in *Proc. British Machine Vision Conference*, vol. 3, 2006, pp. 929–938.
- [24] A. Ashraf, S. Lucey, J. Cohn, T. Chen, Z. Ambadar, K. Prkachin, P. . Solomon, and B.-J. Theobald, "The Painful Face: Pain Expression Recognition using Active Appearance Models," in *Proceedings of the 9th international conference on Multimodal interfaces*. Nagoya, Aichi, Japan: ACM, 2007, pp. 9–14.
- [25] D. J. Field, "Relations between the Statistics of Natural Images and the Response Properties of Cortical Cells," *Journal of the Optical Society of America A*, vol. 4, no. 12, pp. 2379–2393, 1987.
- [26] Y. Lecun, K. Kavukcuoglu, and C. Farabet, "Convolutional Networks and Applications in Vision," in *Proc. International Symposium on Circuits and Systems (ISCAS'10)*, 2010.
- [27] N. Pinto and D. Cox, "Beyond simple features: A large-scale feature search approach to unconstrained face recognition," in *IEEE International Conference on Automatic Face and Gesture Recognition*, 2011.
- [28] N. Pinto, D. Doukhan, and C. D. DiCarlo, J.J., "A High-Throughput Screening Approach to Discovering Good Forms of Biologically-Inspired Visual Representation," *PLoS Computational Biology*, vol. 11, no. 5, p. 2009, 2009.
- [29] A. Berg and J. Malik, "Geometric Blur for Template Matching," in *Computer Vision and Pattern Recognition*, 2001, pp. 607–614.
- [30] M. Bartlett, G. Littlewort, M. Frank, C. Lainscsek, I. Fasel, and J. Movellan, "Fully Automatic Facial Action Recognition in Spontaneous Behavior," in *Proceedings of the International Conference on Automatic Face and Gesture Recognition*, 2006, pp. 223–228.
- [31] G. Littlewort, M. Bartlett, I. Fasel, J. Susskind, and J. Movellan, "Dynamics of Facial Expression Extracted Automatically from Video," *Journal of Image and Vision Computing*, vol. 24, no. 6, pp. 615–625, 2006.
- [32] M. Valstar and M. Pantic, "Fully Automatic Facial Action Unit Detection and Temporal Analysis," in *Computer Vision and Pattern Recognition Workshop CVPRW 06*, Jun. 2006, pp. 149–149.
- [33] C. Cortes and M. Mohri, "Confidence Intervals for the Area Under the ROC curve," *Advances in Neural Information Processing Systems*, 2004.
- [34] J. Fleiss, *Statistical Methods for Rates and Proportions*. Wiley, N.Y, 1981.